Regulatory volume decrease of rat kidney principal cells after successive hypo-osmotic shocks

Sotirios G. Zarogiannis [a,*], Alexander V. Ilyaskin [b], Galina S. Baturina [b], Liubov E. Katkova [b], Dmitriy A. Medvedev [c,d], Denis I. Karpov [c,d], Alexander P. Ershov [c,d], Evgeniy I. Solenov [b,d]

[a] Department of Physiology, Medical School, University of Thessaly, Biopolis, Larissa, Greece
[b] Institute of Cytology and Genetics of the Siberian Branch of the Russian Academy of Sciences, Novosibirsk, Russia
[c] Lavrentyev Institute of Hydrodynamics Siberian Branch of Russian Academy of Sciences, Novosibirsk, Russia
[d] Novosibirsk State University, Novosibirsk, Russia

ARTICLE INFO

ABSTRACT

Outer Medullary Collecting Duct (OMCD) principal cells are exposed to significant changes of the extracellular osmolarity and thus the analysis of their regulatory volume decrease (RVD) function is of great importance in order to avoid cell membrane rupture and subsequent death.

In this paper we provide a sub-second temporal analysis of RVD events occurring after two successive hypo-osmotic challenges in rat kidney OMCD principal cells. We performed experimental cell volume measurements and created a mathematical model based on our experimental results. As a consequence of RVD the cell expels part of intracellular osmolytes and reduces the permeability of the plasma membrane to water. The next osmotic challenge does not cause significant RVD if it occurs within a minute after the primary shock. In such a case the cell reacts as an ideal osmometer. Through our model we provide the basis for further detailed studies on RVD dynamical modeling.

1. Introduction

The renal collecting tubule is the final component of fine control for salt and water homeostasis in all mammals. Thus, it is the key regulator of the extracellular volume and solute composition of the organism. For the most part this process is mediated and regulated through the principal cells of the outer medullary collecting duct (OMCD) that are the main cell population in this part of the kidney epithelium [35]. The importance of this cell population to the whole body homeostasis is critical and evident from the fact that the hereditary disorder Nephrogenic Diabetes Insipidus is associated with a water channel (Aquaporin 2; AQP2) of the principal cells, while Liddle's syndrome is associated with a sodium transporter (amiloride sensitive epithelial sodium channel; ENaC) of the principal cells [2,20].

Since the final composition of the urine is determined in the collecting duct, the cells comprising it are exposed continuously to hyposmotic and hyperosmotic conditions. Therefore it is critical for these cells to maintain their viability and functionality. As a consequence they have adaptive mechanisms regarding their cell volume regulation. The hyposmotic environment causes cell swelling that can disrupt the cell membrane if not counterbalanced. The adaptive mechanism of recovery to cell swelling is termed regulatory volume decrease (RVD) [18]. The series of events in RVD is loss of intracellular osmolytes followed by a rapid concomitant efflux of intracellular water. Thus, the pivotal counterparts of RVD are ion conducting pathways, mainly permeable to K^+, Cl^- and organic anions leading ions out of the cell and water transporting proteins (AQP's) allowing efflux of water along the osmotic gradient [10,18,22,31,33].

Renal principal cells are highly permeable to water since they express three types of AQP's, AQP2 apically and AQP3/AQP4 basolaterally [27]. Water enters cells through the lumen via apical AQP2 and exits to the circulation via basolateral AQP3 and AQP4 [27]. Hypotonicity challenge has been reported to decrease the translocation of AQP2 to the cell surface in order to protect it from excess swelling [34].

Swelling of collecting duct cells may occur very fast and repetitively. Although several attempts have been made to model the RVD of various components of kidney epithelia, little is known about the behavior of cells in conditions of repetitive osmotic changes. Moreover, there are no studies regarding swelling and RVD in cells with fast kinetics of these processes recorded with sub second time resolution. Most mathematical models involve slow exchange processes or steady state modeling of ion and water

* Corresponding author. Address: Department of Physiology, Medical School, University of Thessaly, Biopolis, 41110 Larissa, Greece. Tel.: +30 2410685558; fax: +30 2410685555.
E-mail address: szarog@med.uth.gr (S.G. Zarogiannis).

transport across the cell membrane [1,7,14,15,19,25,39,40]. We have already reported a mathematical modeling approach of fast RVD in kidney epithelia, only for a single hypo-osmotic shock [32], but no modeling approach exists for describing the cell behavior after sequential osmotic shocks. The most adequate way to study such processes is the combination of experimental measurements and mathematical modeling.

The purpose of this work was to study the time course of cell volume changes in principal cells of rat kidney OMCD in hypotonic medium, with high temporal resolution. We provide evidence regarding the changes of ion and water transport governing this cell behavior. Moreover, based on these experiments we opted to construct a mathematical model of this reaction in order to elucidate sub-second cell volume kinetics and RVD processes.

2. Materials and methods

2.1. Animals

All experimental procedures were approved by the Ethical Committee of the Institute of Cytology and Genetics of the Siberian Branch of the Russian Academy of Sciences. Wistar rats weighting 150–200 g (Breeding Laboratory of Experimental Animals, Institute of Cytology and Genetics, Novosibirsk, Russia) were kept in individual cages and received standard diet. For standardization of animals' state and increase of the osmotic water permeability of the OMCD epithelial cells prior to beginning of the experiments, rats were subjected to anti-diuresis by water deprivation and receiving only dry food for 36 h (hypo-hydrated animals).

2.2. Solutions

The solutions used were based on PBS (137 mM NaCl, 4.7 mM Na_2HPO_4, 2.7 mM KCl, 1.5 mM KH_2PO_4, 0.5 mM $MgCl_2$, 1 mM $CaCl_2$, 300 mOsm/l, pH = 7.4) containing 1.0 mg/mL glucose. This solution was chosen in order to be able to degas it without affecting its pH. To create osmotic challenges, bath solutions were changed from normal to PBS diluted with distilled water (1:1). Two subsequent hypotonic challenges were performed with 10–15 s lag.

For medullary substance dispersion calcium-free PBS was used (137 mM NaCl, 4.7 mM Na_2HPO_4, 2.7 mM KCl, 1.5 mM KH_2PO_4, 0.5 mM $MgCl_2$, 0.05 mM $CaCl_2$).

2.3. Collecting duct fragments

Rats were anesthetized by pentobarbital (50 mg/kg intraperitoneally) and decapitated. Extracted kidneys were placed in ice-cold PBS (pH 7.4), then de-capsulated and de-corticated. A suspension of collecting duct fragments was prepared. Tissue from the outer medulla zone was squeezed through a needle (0.45 mm i.d.) in the ice-cold calcium-free PBS. The resulting suspension was filtered through a nylon mesh, diluted 10 times with Eagle MEM culture medium and centrifuged (100 g, 10 min, 4 °C). The sediment containing the tubules was diluted with culture medium to an appropriate concentration of about 10 fragments per μL. This suspension was used in experiments as a preparation of OMCD fragments.

In experiments with hypotonic shock suspension of OMCD fragments was incubated in 0.5 × PBS at 37 °C during 3 min.

2.4. Perfusion chamber and microscopy

A superfusion chamber was constructed as an acrylic block mounted on the objective of an upright microscope (water immersion 65× magnification, numerical aperture 1.1, thermal stabiliza-

tion at 36.8 ± 0.2 °C). The temperature was chosen so as to provide adequate conditions for all transporters and to prevent inhibition of transporters with high energy of activation that could happen at low temperatures [6].

The flow rate of the perfusate was 20 mL/min, which resulted in complete solution exchange in less than 100 ms. Fluorescence measurements of cell volume were performed by the calcein quenching method as it was previously described [30]. Cell volume changes were expressed as relative values of calcein fluorescence. Fragments of outer medullary collecting duct (OMCD) were placed on a glass plate and were loaded with Calcein-AM (Invitrogen, CA, USA) (5.0 μM) by incubation for 15 min at 4 °C, and then for 25 min at 37 °C in 5% CO_2. The glass plate with the fragments of the OMCD was positioned on the stage of a microscope (LOMO-R8, St. Petersburg, Russia). Calcein fluorescence was measured continuously with a halogen light source, through a calcein filter set (480 nm excitation, 490 nm dichroic mirror, 535 nm emission), a photomultiplier detector with a pinhole diaphragm in order to be able to select the cells of interest at the end of the fragment where the both apical and basolateral surface of the cells are exposed to bath solution, and with a 14-bit analog-to-digital converter PCL-818HG (Advantech). The data acquisition rate was 10 ms.

Calcein fluorescence was calibrated by the simultaneous measurements of the fluorescence and the changes of cell height of superfused OMCD fragments challenged by various osmolality of the extracellular medium (150, 300, 400 and 600 mosmol/kgH2O). The superfusion chamber was mounted on the stage of Zeiss Observer Z1 microscope (Zeiss, Germany) (63×, oil immersion, N.A. 1.4) and CCD camera AxioCam HSm (Zeiss, Germany) (frame rate for data acquisition was 10 fps). On the basis of 3D confocal reconstructions in solutions of different osmolalities (see Appendix C), the assumption that OMCD cell volume is proportional to cell height cubed could be accepted: $V/V_0 = (H/H_0)^3$. It is evident from the results of the confocal reconstructions that the osmotically inactive part of the cell volume does not exceed 10% of the total cell volume and thus is small enough to be neglected. The according calibration plot is shown in Fig 1.

2.5. Statistics

Averaged experimental recordings of calcein fluorescence ($n = 5$) were presented as mean value and standard error of mean (M ± SEM).

2.6. Methods of mathematical modeling

In order to construct our model we consider a non-polarized, non-excitable cell expressing water, potassium, sodium, chloride and organic osmolyte channels, Na/K-pump and KCC and NKCC
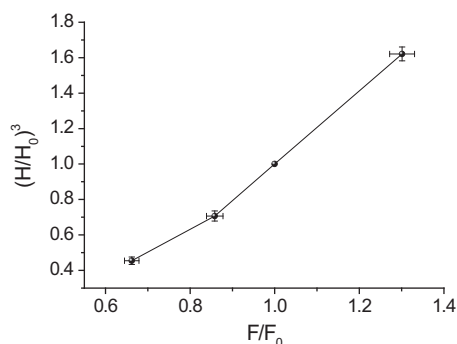

Fig. 1. Calibration plot for the Calcein quenching method. Abscissa: relative Calcein fluorescence; ordinate: relative cell height cubed. All values are presented as M ± SE.

co-transporters in the plasma membrane. The set of membrane osmolyte carriers and transporters implemented in the model is chosen according to expression patterns in collecting duct cells [4,8,9,13,24,26,29,36,37].

The passive ion fluxes through channels were modeled using the Goldman–Hodgkin–Katz expression [12,17]. The activity of Na/K-pump was described by the detailed kinetic scheme using the Hill graphic algorithm [16] as reported previously [3,7,14,15]. The flux through Na/K-pump (J_p) was derived from the kinetic model described in [14,15] using rate constants and other parameters of the Na/K-pump presented in [15]. Since the calculated contribution of the activity of the Na/K-pump in RVD reaction is negligible, in the current model the parameters of Na/K-pump used are the ones obtained by the analysis of Na/K-ATPase in stationary state [14,15].

The contribution of NKCC and KCC cotransporters to the net transmembrane ion flux was estimated experimentally and it was small enough to be neglected ($J_{KCC} = J_{NKCC} = 0$). The estimation that NKCC and KCC activity was negligible was based on the effect of inhibitors of cotransporters on cell volume in isotonic medium. Inhibition of KCC by DIOA (10^{-4} M) (Sigma, Germany) resulted in ~1% increase of cell volume (1.013 ± 0.004, $n = 5$). The effect of NKCC inhibitor bumetanide (10^{-5} M, Sigma, Germany) was undetectable in our experiments ($n = 5$).

E_m was calculated at each time step using the electroneutrality assumption as described in Appendix A. Osmotic water flux was included in the model by the parameter of membrane water permeability (P_w) and the rate of cell volume changes.

To estimate the initial steady state of the model the values of permeability parameters P_{Na}, P_K, P_{Cl} and the Na/K-pump density N, were adjusted so that intracellular $[Na^+]_{in}$, $[K^+]_{in}$ and $[Cl^-]_{in}$ concentrations were in agreement with experimental data for collecting duct cells from previous reports [11,13,28]. Values of P_{Na}, P_K, P_{Cl} were in the range of values taken from the models described previously [41].

Extracellular osmolarity was defined as a sum of the Na^+, K^+ and Cl^- concentrations according to the experimental protocol while the intracellular osmolarity was set as a sum of the Na^+, K^+, Cl^- and hypothetical organic ions' X concentrations.

The amount of organic anions (n_X) was chosen so that the calculated stationary cell volume V was close to the size of OMCD cells ($\sim 1 \times 10^{-9}$ cm^3). The mean charge of organic anions z was set equal to -1.5 according to assumptions made by Fraser [7] to balance steady-state intracellular cation concentrations typical for OMCD cells [11].

The main equations of the model and the initial values of the parameters and variables are listed in Appendix A.

Numerical integration of all foregoing differential equations was carried out by the fourth order Runge–Kutta method. The integration step (dt) was equal to 10^{-2} s. When the simulation was repeated using the ten times smaller integration step (10^{-3} s), no significant changes were observed.

Fitting of the model parameters of water and ion permeabilities was made manually (trial method) or using the Genetic optimization algorithm (GA) (see below) using the criterion of concordance (Eq. (1)) between experimental and model relative total cell volume time course at each time point:

$$\sum_i \left(\left(\frac{V}{V_0} \right)_i^{exp} - \left(\frac{V}{V_0} \right)_i^{calc} \right)^2 = \min. \tag{1}$$

2.7. Genetic optimization algorithm

To find the best-fit values of the model parameters, a Genetic optimization algorithm (GA) was used [42]. For the *first approximation volume-controlled model* (FAVM) the best-fit values of the fol-

lowing parameters were obtained: (1) $V_{threshold}$, (2) *gain* and (3) P_X^{RVD} and for the *second approximation volume-controlled model* (SAVM): (1) μ, (2) *gain* and (3) P_X^{RVD} (see Appendix B and Table B for details). The best-fit values of the model parameters correspond to the minimum of the function defined by Eq. (1) (minimization function F).

GA is a heuristic algorithm based on a random choice of parameter values from the specified range and a goal-directed selection of the best-fit variants. The optimization procedure starts when the initial set of M vectors of the model parameters [for FAVM this vector corresponds to the set of three parameter values ($V_{threshold}$, *gain*, P_X^{RVD}), for SAVM – (μ, *gain*, P_X^{RVD})] is generated, where $M = 20$. Each parameter value was randomly chosen from the following range:

$$V_{threshold} : \; (1.0 - 1.8),$$

$$gain : \; (1 - 10),$$

$$P_X^{RVD} : \; (0 - 1.0 \times 10^{-4} \text{ cm/s}),$$

$$\mu : \; (0.1 - 0.8).$$

Each vector is referred to as an "individual" and a set of M vectors is named as a "population".

For each "individual" of the "population", the reaction of a cell to a hypotonic shock was simulated, and the concordance between experimental and simulated time curves for the relative total cell volume at each time point was calculated using Eq. (1) [that was the value of minimization function (F)]. The values of the model parameters that corresponded to the best-fit "individual" were saved as the result of the initial run of GA. Then "individuals" of the initial "population" were sorted according to the values of F and only half ($M/2$) of the "individuals" having the minimal values of F was kept. The remaining half of the "population" was generated by the so-called "mating" procedure. The selected $M/2$ "individuals" formed pairs: i_n with i_{n+1}; i_{n+2} with i_{n+3} etc. and exchanged their parameter values according to the following scheme forming a pair of new "individuals":

$$i_n \left(p_n^1, p_n^2, p_n^3 \right) + i_{n+1} \left(p_{n+1}^1, p_{n+1}^2, p_{n+1}^3 \right)$$
$$= i_{n+M/2} \left(p_n^1, p_n^2, p_{n+1}^3 \right) + i_{n+M/2+1} \left(p_{n+1}^1, p_{n+1}^2, p_n^3 \right).$$

The last procedure of the each round of GA was the "mutation" of parameter values. For each "individual" i_n $\left(p_n^1, p_n^2, p_n^3 \right)$ one of the parameters was randomly selected p_n^j, where $j = 1$, 2 or 3. Its value was changed according to the formula: $p_n^{j,new} = p_n^j (1 + 0.4 \cdot r)$, where r – a random variable having the uniform distribution in the range [-0.5 to 0.5]. The use of "mutation" allows one to avoid local minima and to move beyond the initially specified ranges of parameter values if the global minimum does not lie within those ranges.

When all the procedures ("selection", "mating", "mutation") are completed we obtain the new "population" of "individuals" ready for a new round of GA.

Optimization of the values of the model parameters using GA was repeated until the value of the minimization function F for each "population" (determined by the best-fit "individual" in the "population") reached a plateau at the minimum level. Finally, the best-fit values of the model parameters were obtained as $M \pm SEM$ by averaging of their values correspondent to the plateau of the F function.

We also proved the efficiency of the Genetic Algorithm of optimization using the test function dependent on five parameters to be fitted. In the range of function parameters' variation the function had 243 minima and only one was the global minimum. When the number of "individuals" in the "population" was small (<10),

GA reached one of the local minima with the probability nearly equal to 0.5. Increasing the size of the "population" (20–30 "individuals") allowed us to obtain the solution that corresponded to the global minimum of the test function.

3. Results and discussion

3.1. Experimental measurements of cell volume changes under the influence of two successive hyposmotic shocks in rat principal cells of OMCD

Fig. 2 represents the time course of the relative cell volume changes of principal cells under the influence of two successive hypotonic shocks. The hypotonic challenge results in an increase of the cell volume that is followed by RVD reaction leading to recovery of the initial cell volume. In hypotonic conditions, the cell volume can decrease only due to the flux of osmotically active substances out of the cell. Therefore, the equilibrium cell volume after the return to normotonic medium is reduced to approximately 50% of the initial cell volume. This value is in a good agreement with the fact that the most cell volume is osmotically active (See Appendix C). The subsequent hypotonic challenge that takes place 10–15 s after the end of the primary hypotonic shock leads to cell volume change resembling the behavior of an ideal osmometer. In addition there is only minor reduction in the stable level of the cell volume in normotonic conditions after the end of the second shock indicating that the most significant loss of osmolytes takes place during the first hypotonic challenge.

Parts of the calcein fluorescence signal that correspond to cell volume changes in cases of the primary hypotonic shock, return to normotonicity and the subsequent hypotonic shock were fitted by the exponential function:

$$\frac{V}{V_0} = A + B \exp\left(-\frac{t - t_0}{\tau}\right) \tag{2}$$

Here A and B are constants, $t - t_0$ is the time measured from the start of the shock. Parameter τ is the characteristic time of cell volume increase or decrease. Three such parameters were calculated ($\tau_1 = 0.31 \pm 0.16$; $\tau_2 = 1.22 \pm 0.02$; $\tau_3 = 1.54 \pm 0.05$ s; $p < 0.01$) for the first swelling in hypotonic conditions, shrinkage in normotonic conditions and the second hypotonic challenge, respectively. The cell shrinkage in normotonic conditions after the first hypotonic shock and the swelling when the second hypotonic shock is applied are substantially slower than the first swelling, which means
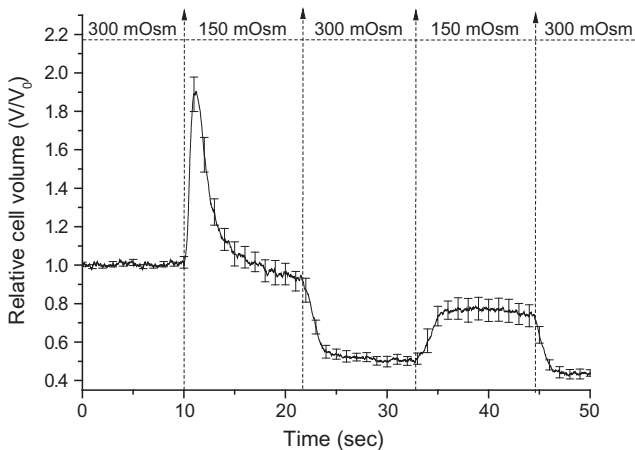
that the membrane water permeability is notably decreased. Evidently, such change in the cell response to the second hypotonic shock is the result of the activation of protective mechanisms during the primary hypotonic challenge.

The estimated values of the membrane water permeabilities were found by manually fitting the experimental curves to minimize the value of Eq. (1) (see Section 2.6):

during first swelling in hypotonic conditions: $P_w = 1.2 \times 10^{-1}$ cm/s;

during shrinkage in normotonic conditions: $P_w = 1.2 \times 10^{-2}$ cm/s;

during subsequent swelling in hypotonic conditions: $P_w = 1.2 \times 10^{-2}$ cm/s.

These values produce the best agreement between the model described further and the experimental data. The decrease of P_w parameter was modeled as shown in Appendix B. So, the experimental data suggest that the osmotic water permeability decreases by factor of ten, under the first influence of the hypotonicity and remains reduced during the second subsequent shock. This finding reflects probably the cell adaptation after the first hypotonic shock as it reduces the risk of cell damage under the hypotonic challenge. In addition, it is in agreement with the fact that hypotonicity challenge has been reported to decrease the translocation of AQP2 to the cell surface in order to protect it from excess swelling [34].

3.2. Mathematical modeling of the relative cell volume changes of principal cells under the influence of two successive hypotonic shocks

On the basis of foregoing experimental data a mathematical model of the cell reaction to the hypotonic shocks of a rat principal cell of the OMCD was constructed. A detailed description of the equations and the initial values of variables and parameters used are provided in Appendix A. It was accepted that the whole cell volume is involved in osmosis. The model employs the relative cell volume as a trigger for RVD activation. The modifications of the model are described in detail in Appendix B.

The model was developed in two steps. Each successive modification improved the approximation by introducing new adjustable parameters. The decrease in water permeability mentioned above was taken into account by applying a tenfold reduction of the P_w coefficient (Appendix B).

Initially we accepted a simple mechanism of RVD which was modeled by an abrupt increase of K^+, Cl^- and organic osmolytes' (X) fluxes out of the cell. As the cell volume exceeded a certain threshold level ($V_{threshold}$), the P_K^0 and P_{Cl}^0 membrane permeabilities were multiplied by a parameter that we called "gain". Simultaneously the organic anions (X) were allowed to escape the cell, i.e. the permeability of the plasma membrane for these ions termed P_X, increased from zero to the value equal to the $P_X = P_X^{RVD}$ (not multiplied by gain). When the relative cell volume decreased again to the same threshold level, the initial values of permeability parameters were restored. Using the genetic optimization algorithm the best-fit values of the model parameters were obtained: $V_{threshold} = 1.096 \pm 0.001$, $P_X^{RVD} = 1.61 \times 10^{-5} \pm 0.03 \times 10^{-5}$ cm/s, gain = 3.09 ± 0.06. This primary level of the model is called first approximation volume-controlled model (FAVM). It can be noticed from the simulated cell volume time dependence, that FAVM simulates the real cell behavior rather poorly (the value of Eq. (1) is 1.3×10^1) (Fig. 3). Particularly there are significant deviations in the magnitude of peak volume. Note the good agreement during the interval 22–33 s (return to normotonicity).

For further improvement of the model, a lag period (τ_{lag}) of adaptive increase of the permeability parameters was introduced

Fig. 2. Time course of the relative cell volume V/V_0 of renal OMCD principal cells affected by two consecutive hyposmotic shocks. Relative cell volume (V/V_0) obtained from averaged experimental recordings of calcein fluorescence fluctuations and calibration plot (Fig. 1) (M ± SEM; $n = 5$). The top scale represents the changes of the osmolarity of the extracellular medium in mOsm.
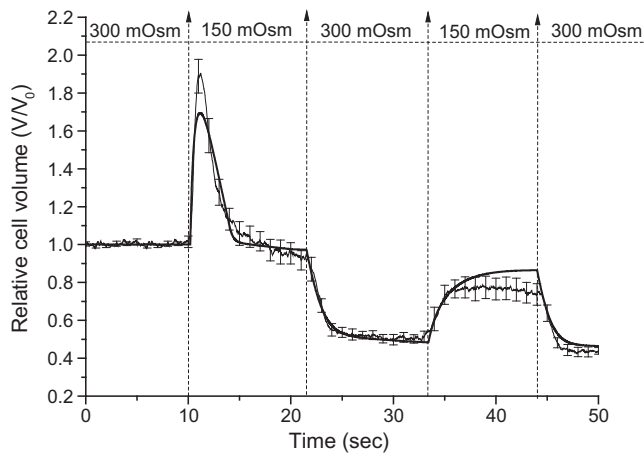
Fig. 3. Simulation of RVD reaction employing the first approximation model (FAVM). The time dependence of the relative cell volume is plotted (V/V_0) [solid bold line – model; solid thin line – experiment]. The top scale represents the changes of the osmolarity of the extracellular medium in mOsm.

in the model. Experimental data showed that at the beginning of the cell swelling (first 0.9–1 s) the cell increases its volume like an ideal osmometer indicating that there is no significant osmolyte efflux during this time. Taking into consideration this observation the lag period between the change of extracellular osmolarity and the launch of RVD reaction was set to 1 s. Also the continuous dependence of the permeability on cellular volume was adopted. In this modification the increase of membrane ion permeability parameters was expressed by the continuous function $f(V/V_0)$ containing the adjustable parameter μ (see Appendix B). Such dependence reflects the gradual response of the cell to the osmotic volume perturbation that is natural within the mechanical activation concept. The actual form of function (parabolic) was chosen from considerations of simplicity as well as reproduction of the experimental data. One should note that in simulations this function is limited by the RVD reaction. To reduce the number of parameters to be fitted the threshold level $V_{threshold}$ was set to 1.0 as in the FAVM modification of the model this parameter was close to unity.

Using the genetic optimization algorithm the following best-fit values of parameters were obtained: $P_X^{RVD} = 2.923 \times 10^{-5} \pm 0.065$ -

$\times 10^{-5}$ cm/s, $gain = 1.313 \pm 0.008$ and $\mu = 0.319 \pm 0.003$. The calculations showed that continuous modification of the model (called the *second approximation*, SAVM) was satisfactory enough to reproduce the behavior of the real cell. One can see that the value of fitting Eq. (1) was decreased significantly in comparison with previous step (the value of Eq. (1) is 8.8) (Fig. 4).

Our study reveals some very important characteristics of the process of RVD. More specifically, we provide novel information regarding the time course of the cell volume corresponding to RVD at the sub-second scale, as well as the potential adaptive reaction of OMCD principal cells in the successive hypotonic shock.

High levels of ion permeabilities are essential for RVD. If the permeabilities for K$^+$ and Cl$^-$ are high enough like in OMCD cells [40] the RVD reaction could be accomplished by the increasing permeability of organic osmolytes only even if the permeabilities for K$^+$ and Cl$^-$ remained unchanged as it is for $gain = 1$. Without the significant organic efflux RVD is attenuated even if P_K and P_{Cl} are increased (Fig. 5). The analysis of the osmolyte fluxes in SAVM model corroborated the conventional perspective that the RVD is mainly performed by significant release of K$^+$ and organic anions out of the cell (J_K and J_X). The mathematical modeling allowed us to estimate the contribution of different ion fluxes to the cell volume decrease (Fig. 6a–c). The significant depolarization of the membrane predicted by the model, accounts for the limited efflux of negatively charged ions. Note that the prevention of significant depolarization when $gain = 5$ (when P_X increase is accompanied by the increase of $P_K + P_{Cl}$) promoted the loss of ions by a model cell.

In many cell types it was shown that the role of K$^+$ and Cl$^-$ efflux is crucial for RVD [18,22]. We examined the possible effect of K$^+$ and Cl$^-$ efflux to RVD using the SAVM model where the organic efflux was set to zero ($P_X = 0$), so RVD was carried out by increasing P_K and P_{Cl} by a $gain = 10$. Analysis of the model suggests that the efficiency of RVD is dependent on the chloride cell content. The intracellular content of Cl$^-$ is greatly influenced by the balance of two cotransporters: KCC and NKCC. However, it should be noted that as cotransporters are not active in OMCD principal cells, intracellular chloride is passively distributed across the plasma membrane and its value is defined by the transmembrane electric potential difference. To increase the steady state intracellular Cl$^-$ concentration in the model cell one has to increase the ratio of permeability parameters (P_{Na}/P_K). For example, if the values of permeability parameters were as follows: $P_{Na} = 5.0 \times 10^{-6}$ cm/s,
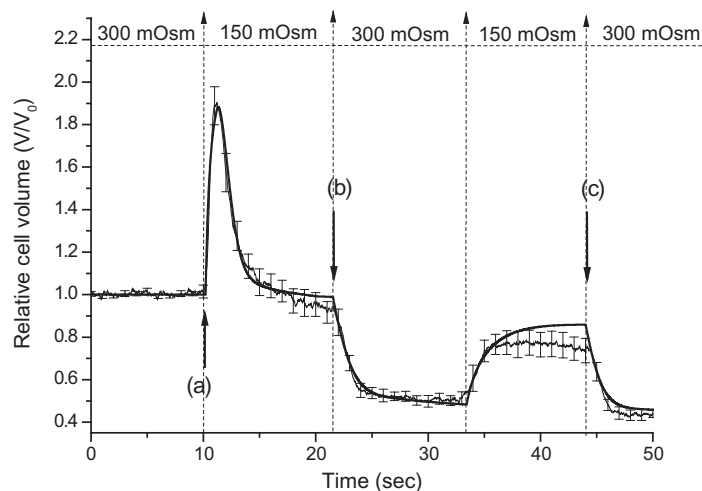

Fig. 4. Simulation of RVD reaction employing the second approximation model (SAVM). The time dependence of the relative cell volume is plotted (V/V_0) [solid bold line – model; solid thin line – experiment]. The top scale represents the changes of the osmolarity of the extracellular medium in mOsm. Arrows (a), (b) and (c) correspond to the columns of Table 1.
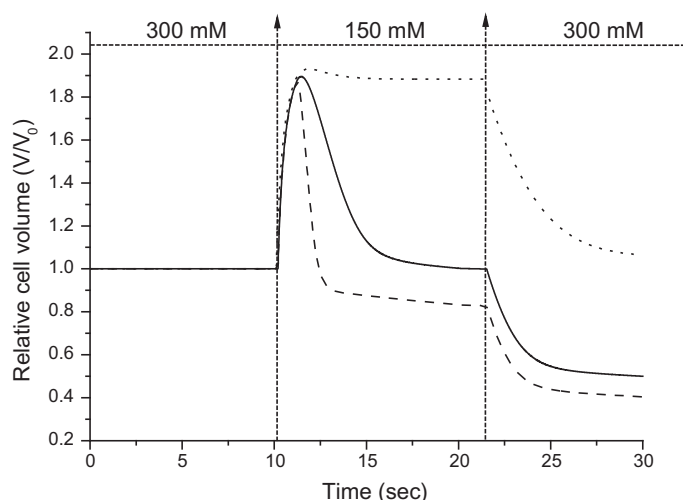
Fig. 5. Simulation of RVD reaction employing the second approximation model (SAVM) with different patterns of permeability increase. The time dependence of the relative cell volume (V/V_0) is plotted. Solid line – P_X was increased (*gain* = 1); dashed line – P_X and $P_K + P_{Cl}$ were increased (*gain* = 5); dotted line – $P_K + P_{Cl}$ were increased with *gain* = 5, P_X remains zero. The top scale represents the changes of the total concentration of extracellular osmolytes in mM.

$P_K = 2.0 \times 10^{-5}$ cm/s the initial steady state value of $E_m = -0.046$ V and the Cl$^-$ cell content was increased ($[Cl^-]_{in} = 27$ mM). We simulated three levels of intracellular Cl$^-$ concentrations, namely 14, 27 and 41 mM. The increase of the permeability parameters for K$^+$ and Cl$^-$ without increasing the permeability for organic anions produces too weak RVD though it becomes more effective if the Cl$^-$ cell content is increased (Fig. 7). It is readily seen that even at 41 mM of Cl$^-$, which is probably too high for OMCD cells, the efflux of even all Cl$^-$ and equivalent K$^+$ without efflux of organic anions would be insufficient to produce the RVD observed experimentally.

The RVD reaction during the second hypotonic shock remained practically inactive and the cell behavior resembled the behavior of an ideal osmometer. The slower swelling was a consequence of decreased water permeability that can be considered as an adaptive reaction to the extracellular hypotonic environment. The calculated changes of intracellular concentrations (mol/cm^3) and amounts (mol/cell) of osmolytes during the simulation are displayed in Table 1 (the correspondent time points are indicated in Fig. 4). Analysis of the model shows that the amounts of Na$^+$, K$^+$ and organic anions are reduced about 50% after the first shock (Table 1). In the second hypotonic shock the efflux of cellular osmolytes was reduced by a factor of ten. The above indicate that the main body of osmolyte loss occurs predominantly under the first osmotic challenge.

More importantly we managed to show for the first time that after the first hypotonic shock the water permeability of the OMCD cells decreases rapidly though the mechanism remains undetermined. However, our data are supported by previously demonstrated internalization of AQP2 under hypotonic conditions [34]. Probably internalization of AQP2 water channels is one of the key processes in RVD. Cells swell slower and the RVD reaction is weaker during the second hypotonic shock. This is reflected in the model equations by the tenfold decrease in the water permeability. Our experimental and theoretical results regarding the cell response to the changes of the extracellular osmolarity show that the alterations of cell properties have adaptive nature.

4. Concluding remarks

Herein, we report experimental data and mathematical modeling simulation of the RVD processes of OMCD principal cells under the influence of two successive hypotonic shocks. To our knowledge, this is the first model of RVD based on experimentally measured time course of the relative cell volume involving sub-second time resolution since all other models involve slow exchange processes or steady state modeling [1,7,14,15,19,25,39,40]. At the second shock the water permeability of the cell was reduced and the ion osmolyte loss was equally reduced. It is possible that the process responsible for the decrease of water permeability is apical AQP2 and/or basolateral AQP3 and AQP4 internalization. These assumptions require experimental verification. Particularly it is necessary to study the molecular mechanisms underlying the rapid decrease of membrane water permeability of cells.

It is necessary to take into account that there are several kinds of stretch-activated ion channels on the cell surface [5,38] and that the mechanical tension of the cytoskeleton may affect signal transduction pathways: certain kinases and G-proteins could be involved in this reaction [21,23]. Pure mechanical activation that was used up to now in our model cannot by itself reflect the variety of processes that take place in the cell during the hypotonic shock. Biochemical processes which may be triggered by changes of the cell volume, intracellular ion concentrations and electric membrane potential are at least of no less importance. Conclusions made on the basis of mathematical modeling of the cell response to hypotonic shocks allow us to speculate about the processes of cell adaptation to hypotonicity.

5. Disclosure statement

The authors of this manuscript have nothing to disclose.

Appendix A. Variables, parameters and equations of the mathematical model

In the current work the transmembrane diffusion fluxes of Na$^+$, K$^+$, Cl$^-$ and organic anions X along with the Na/K-pump activity
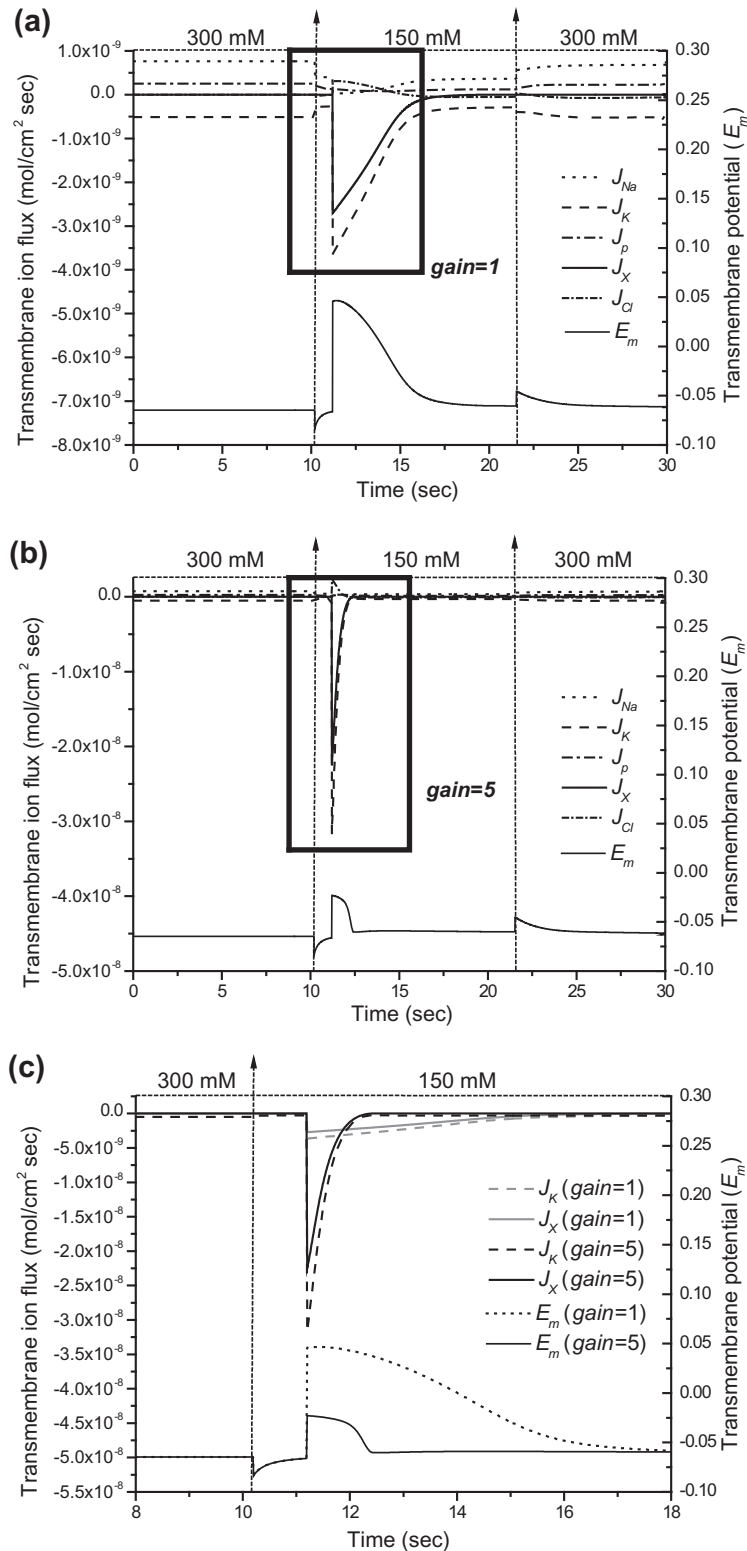
Fig. 6. The time dependence of simulated transmembrane ion fluxes (mol/cm^2 sec) and transmembrane potential difference E_m (V) during the first hypotonic shock in SAVM model. (a) General ratio of fluxes through different membrane transporters and potential difference E_m profile (gain = 1); (b) general ratio of fluxes through different membrane transporters and potential difference E_m profile (gain = 5); (c) scaled-up part of the (a) and (b) graphs (marked by rectangular frame) representing J_X and J_K fluxes and potential difference E_m profile. The top scale represents the changes of the total concentration of extracellular osmolytes in mM. Note, that fluxes of Na$^+$ and K$^+$ provided by Na/K-ATPase activity are equal to $-3J_p$ and $2J_p$, respectively.

were modeled (the ion fluxes through KCC and NKCC cotransporters were set to zero). The cell surface area A through which transport of osmolytes and water occurs remained constant and independent of cellular volume changes (see Table A1).

The following equations describe the flux of water causing the changes in the cell volume V, fluxes of osmolytes Na$^+$, K$^+$, Cl$^-$ and of organic anions X (in mole), and the time dependence of electric transmembrane potential difference (E_m):
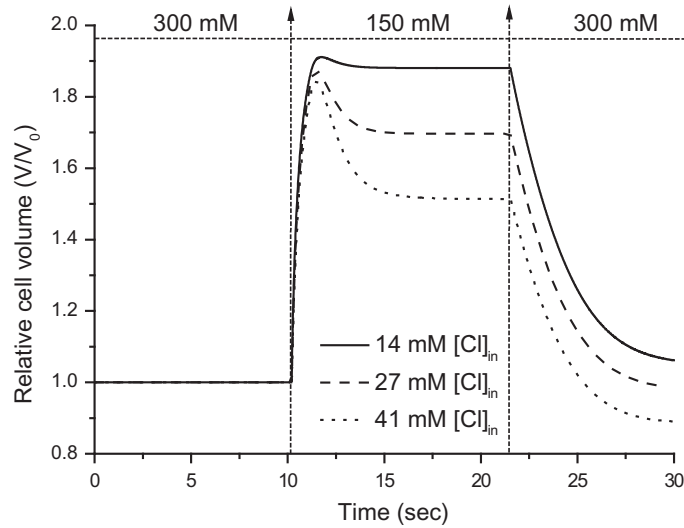
Fig. 7. Simulation of RVD reaction employing the second approximation model (*SAVM*) where the organic efflux was set to zero ($P_X = 0$) and $P_K + P_{Cl}$ were increased (*gain* = 10). Effect of the difference in intracellular Cl^- content to RVD. The time dependence of the relative cell volume (V/V_0) is plotted {solid line – $[Cl^-]_{in}$ = 14 mM (P_{Na} = 2.0 × 10^{-6} cm/s; P_K = 2.0 × 10^{-5} cm/s); dashed line – $[Cl^-]_{in}$ = 27 mM (P_{Na} = 5.0 × 10^{-6} cm/s; P_K = 2.0 × 10^{-5} cm/s); dotted line – $[Cl^-]_{in}$ = 41 mM (P_{Na} = 8.0 × 10^{-6} cm/s; P_K = 2.0 × 10^{-5} cm/s)}. The top scale represents the changes of the total concentration of extracellular osmolytes in mM.

Table 1
Simulated values of the intracellular concentration (mol/cm^3) and the amount (mol/cell) of osmolytes before (a) and at the end of the first (b) and the subsequent (c) hypotonic shock. See Fig. 4 where the correspondent time points are indicated by arrows.

	Intracellular concentration (mol/cm^3)			Intracellular amount (mol/cell)		
	Before the first shock (a)	At the end of the first shock (b)	At the end of the subsequent shock (c)	Before the first shock (a)	At the end of the first shock (b)	At the end of the subsequent shock (c)
Na$^+$	1.37 × 10^{-5}	6.48 × 10^{-6}	6.68 × 10^{-6}	1.38 × 10^{-14}	6.42 × 10^{-15}	5.74 × 10^{-15}
K$^+$	1.64 × 10^{-4}	7.93 × 10^{-5}	8.14 × 10^{-5}	1.65 × 10^{-13}	7.86 × 10^{-14}	7.00 × 10^{-14}
Cl$^-$	1.34 × 10^{-5}	1.74 × 10^{-5}	9.32 × 10^{-6}	1.34 × 10^{-14}	1.73 × 10^{-14}	8.01 × 10^{-15}
X	1.09 × 10^{-4}	4.55 × 10^{-5}	5.25 × 10^{-5}	1.10 × 10^{-13}	4.51 × 10^{-14}	4.51 × 10^{-14}
Total	3.00 × 10^{-4}	1.49 × 10^{-4}	1.50 × 10^{-4}	3.00 × 10^{-13}	1.47 × 10^{-13}	1.29 × 10^{-13}

$$\frac{dV}{dt} = AV_W P_W \left(([Na^+]_{in} + [K^+]_{in} + [Cl^-]_{in} + [X]_{in}) - \Pi_e \right); \tag{A1}$$

$$\frac{dn_{Na}}{dt} = A[-3J_p + J_{Na} + J_{NKCC}]; \tag{A2}$$

$$\frac{dn_K}{dt} = A[2J_p + J_K + J_{KCC} + J_{NKCC}]; \tag{A3}$$

$$\frac{dn_{Cl}}{dt} = A[J_{Cl} + 2J_{NKCC} + J_{KCC}]; \tag{A4}$$

$$\frac{dn_X}{dt} = AJ_X; \tag{A5}$$

In order to obtain the time dependence of membrane potential E_m, we employed a stationary solution of the electroneutral condition:

$$-J_p + J_{Na} + J_K - J_{Cl} + zJ_X = 0 \tag{A6}$$

using the same approach as it was previously described [15]. For the explicit formula for E_m calculation see Eq. (A12) below.

Passive ion fluxes were modeled as follows [12,17]:

$$J_{Na} = P_{Na}\varepsilon(u)\left[[Na^+]_{out}exp\left(-\frac{u}{2}\right) - [Na^+]_{in}exp\left(\frac{u}{2}\right) \right]; \tag{A7}$$

$$J_K = P_K\varepsilon(u)\left[[K^+]_{out}exp\left(-\frac{u}{2}\right) - [K^+]_{in}exp\left(\frac{u}{2}\right) \right]; \tag{A8}$$

$$J_{Cl} = P_{Cl}\varepsilon(u)\left[[Cl^-]_{out}exp\left(\frac{u}{2}\right) - [Cl^-]_{in}exp\left(-\frac{u}{2}\right) \right], \tag{A9}$$

where $u = FE_m/RT$ and $\varepsilon(u) = u/[exp(u/2) - exp(-u/2)]$.

The outward flux of organic anions is defined similarly taking into account that their extracellular concentration $[X]_{out} = 0$:

$$J_X = -P_X\varepsilon(uz)\left[[X]_{in} \exp\left(\frac{uz}{2}\right) \right]. \tag{A10}$$

The Na$^+$/K$^+$-pump activity was described by the detailed kinetic scheme that is reported in [3,7,14,15] and calculates the pump flux J_p as:

$$J_p = N\frac{\alpha - \beta}{\sum} \tag{A11}$$

where N is the membrane pump density, α is the function of forward rate constants:

$$\alpha = a_{12}a_{23}a_{34}a_{45}a_{56}a_{61}$$

$$a_{12} = f_{12}[Na^+]_{in}^3$$
$$a_{23} = f_{23}$$
$$a_{34} = f_{34}$$
$$a_{45} = f_{45}[K^+]_{out}^2$$
$$a_{56} = f_{56}[ATP]_{in}$$
$$a_{61} = f_{61}$$

β is the function of backward rate constants:

$$\beta = a_{21}a_{32}a_{43}a_{54}a_{65}a_{16}$$

$a_{21} = b_{21}$

$a_{32} = b_{32}[ADP]_{in}$

$a_{43} = b_{43}[Na^+]^3_{out}$

$a_{54} = b_{54}[P_i]_{in}$

$a_{65} = b_{65}$

$a_{16} = b_{16}[K^+]^2_{in}$

and Σ is the function of all rate constants and the ligand concentrations implemented in the kinetic scheme [14]:

$\Sigma = A_1 + A_2 + A_3 + A_4 + A_5 + A_6$

$A_1 = a_{23}a_{34}a_{45}a_{56}a_{61} + a_{34}a_{45}a_{56}a_{61}a_{21} + a_{45}a_{56}a_{61}a_{21}a_{32}$
$\quad + a_{56}a_{61}a_{21}a_{32}a_{43} + a_{61}a_{21}a_{32}a_{43}a_{54} + a_{21}a_{32}a_{43}a_{54}a_{65}$

$A_2 = a_{12}a_{34}a_{45}a_{56}a_{61} + a_{12}a_{45}a_{56}a_{61}a_{32} + a_{12}a_{56}a_{61}a_{32}a_{43}$
$\quad + a_{12}a_{61}a_{32}a_{43}a_{54} + a_{12}a_{32}a_{43}a_{54}a_{65} + a_{32}a_{43}a_{54}a_{65}a_{16}$

$A_3 = a_{12}a_{23}a_{45}a_{56}a_{61} + a_{12}a_{23}a_{56}a_{61}a_{43} + a_{12}a_{23}a_{61}a_{43}a_{54}$
$\quad + a_{12}a_{23}a_{43}a_{54}a_{65} + a_{23}a_{43}a_{54}a_{65}a_{16} + a_{21}a_{43}a_{54}a_{65}a_{16}$

$A_4 = a_{12}a_{23}a_{34}a_{56}a_{61} + a_{12}a_{23}a_{34}a_{61}a_{54} + a_{12}a_{23}a_{34}a_{54}a_{65}$
$\quad + a_{23}a_{34}a_{54}a_{65}a_{16} + a_{34}a_{21}a_{54}a_{65}a_{16} + a_{21}a_{32}a_{54}a_{65}a_{16}$

$A_5 = a_{12}a_{23}a_{34}a_{45}a_{61} + a_{12}a_{23}a_{34}a_{45}a_{65} + a_{23}a_{34}a_{45}a_{65}a_{16}$
$\quad + a_{34}a_{45}a_{21}a_{65}a_{16} + a_{45}a_{21}a_{32}a_{65}a_{16} + a_{21}a_{32}a_{43}a_{65}a_{16}$

$A_6 = a_{12}a_{23}a_{34}a_{45}a_{56} + a_{23}a_{34}a_{45}a_{56}a_{16} + a_{34}a_{45}a_{56}a_{21}a_{16}$
$\quad + a_{45}a_{56}a_{21}a_{32}a_{16} + a_{56}a_{21}a_{32}a_{43}a_{16} + a_{21}a_{32}a_{43}a_{54}a_{16}.$

The rate constants f_{34} and b_{43} are assumed to depend on the value of membrane potential E_m [15]:

$f_{34} = f^0_{34} \exp(FE_m/2RT)$

$b_{43} = b^0_{43} \exp(-FE_m/2RT).$

Since one working cycle of Na/K-pump includes the transfer of three Na^+ out and two K^+ in a cell, the fluxes of Na^+ and K^+ provided by ATPase activity equal $-3J_p$ and $2J_p$, respectively.

Using the expressions (Eq. (A7))–(Eq. (A10)) describing passive Na^+, K^+, Cl^- organic anions' fluxes and the formulation for the flux through Na/K-pump (Eq. (A11)) (see above) the following expression for E_m can be derived:

Table A1
Symbols of parameters and variables used in the model.

Parameter/variable	Symbol
Cell volume	V
Cell surface area	A
Integration step	dt
Membrane Na^+ permeability	P_{Na}
Membrane K^+ permeability	P_K
Membrane Cl^- permeability	P_{Cl}
Membrane X permeability	P_X
Membrane osmotic water permeability	P_w
Intracellular concentration and amount of Na^+, respectively	$[Na^+]_{in}, n_{Na}$
Intracellular concentration and amount of K^+	$[K^+]_{in}, n_K$
Intracellular concentration and amount of Cl^-	$[Cl^-]_{in}, n_{Cl}$
Intracellular concentration and amount of organic anions X	$[X]_{in}, n_X$
Transmembrane potential difference	E_m
Total Na/K-pump membrane density	N
Extracellular Na^+ concentration	$[Na^+]_{out}$
Extracellular K^+ concentration	$[K^+]_{out}$
Extracellular Cl^- concentration	$[Cl^-]_{out}$
Total extracellular concentration of osmolytes	Π_e
Mean organic osmolyte valency	z
Partial molar volume of water	V_w
Faraday's constant	F
Absolute temperature	T
Gas constant	R

According to the experimental conditions, the hypotonic shock was modeled by decreasing twofold the values of extracellular concentrations, i.e. $[Na^+]_{out}/2$, $[K^+]_{out}/2$, $[Cl^-]_{out}/2$. The fitting of the values of the model parameters was performed in a way that would maximize the correspondence between averaged experimental and simulated data points of the relative cell volume time course using the Eq. (1).

Appendix B. Specification of the model approximations used

The reaction of regulatory volume decrease (RVD) was modeled by triggering the complex of regulatory events that included increase of membrane permeability to K^+ and Cl^- ions and outward flux of organic anions X.

In all cases the water permeability also varied: when $t > 10$ s, $P_w = P^0_w/10$, where t starts at the moment of first osmolarity change (300 mM → 150 mM).

For the Second approximation (SAVM) RVD process begins after a lag time ($t > \tau_{lag}$, $\tau_{lag} = 1$ s), where t starts at the moment of first osmolarity change (300 mM → 150 mM). The best-fit values of

$$E_m = \frac{RT}{F} \ln \left(\frac{(P_{Na}[Na^+]_{out} + P_K[K^+]_{out} + P_{Cl}[Cl^-]_{in})\varepsilon(u) + \frac{N}{\Sigma}a_{21}a_{32}b^0_{43}[Na^+]^3_{out}a_{54}a_{65}a_{16} - zP_X[X]_{in}\varepsilon(uz)\exp\left(\frac{u(1+z)}{2}\right)}{(P_{Na}[Na^+]_{in} + P_K[K^+]_{in} + P_{Cl}[Cl^-]_{out})\varepsilon(u) + \frac{N}{\Sigma}a_{12}a_{23}f^0_{34}a_{45}a_{56}a_{61}} \right), \tag{A12}$$

where u and $\varepsilon(u)$ are the same as in Eqs. (A7), (A8), (A9), (A10).

This transcendental equation was solved by iteration method. The next approximation was found as the right-hand part computed using the previous approximation. The iterations were stopped when two successive values differed by less than 10^{-10} V.

The contribution of NKCC and KCC cotransporters to the net transmembrane ion flux was estimated experimentally and it was small enough to be neglected. Under assumption that the contribution of KCC and NKCC cotransporters to the total transmembrane flux is insignificant the corresponding fluxes in the model were set equal to zero: $J_{KCC} = J_{NKCC} = 0$.

The initial values of the main model parameters are listed in Table A2 and the values of parameters of the Na/K-pump are shown in Table A3.

$V_{threshold}$, gain and P^{RVD}_X for FAVM and values of $V_{threshold}$, gain, P^{RVD}_X and μ for SAVM were obtained using the genetic optimization algorithm as described in Materials and Methods (Section 2.7).

Appendix C. 3D confocal reconstructions of cultured principal OMCD cells in solutions with different osmolalities

The primary culture of OMCD cells was grown on cover glass, stained with CellMask Orange (Invitrogen, USA) and placed in the flow chamber on the stage of a laser scanning microscope Zeiss LSM 780 (Zeiss, Germany) (Alfa Plan Apochromat 100× Oil DIC M27, N.A. 1.46, zoom 0.8, scan mode: scaling X and Y: 0.21 μm, Z: 0.17 μm, wavelength 561 nm 2.0%). 3D confocal reconstructions were performed in solutions having osmolalities 300, 400,

Table A2
Initial values of parameters and variables used in the model of collecting duct principal cell.

Parameter	Symbol	Value
Cell volume	V	1×10^{-9} cm^3
Cell surface area	A	1×10^{-5} cm^2
Membrane Na$^+$ permeability	P_{Na}	2×10^{-6} cm/s
Membrane K$^+$ permeability	P_K^0	2×10^{-5} cm/s
Membrane Cl$^-$ permeability	P_{Cl}^0	2×10^{-6} cm/s
Membrane X permeability	P_X^0	0 cm/s
Membrane osmotic water permeability	P_w^0	1.2×10^{-1} cm/s
Intracellular Na$^+$ concentration	$[Na^+]_{in}$	1.37×10^{-5} mol/cm^3
Intracellular K$^+$ concentration	$[K^+]_{in}$	1.64×10^{-4} mol/cm^3
Intracellular Cl$^-$ concentration	$[Cl^-]_{in}$	1.34×10^{-5} mol/cm^3
Intracellular amount of organic anions	n_X	1.1×10^{-13} mol/cell
Transmembrane potential difference	E_m	-0.065 V
Total Na/K-pump membrane density	N	3×10^{-11} mol/cm^2
Extracellular Na$^+$ concentration	$[Na^+]_{out}$	1.45×10^{-4} mol/cm^3
Extracellular K$^+$ concentration	$[K^+]_{out}$	5×10^{-6} mol/cm^3
Extracellular Cl$^-$ concentration	$[Cl^-]_{out}$	1.5×10^{-4} mol/cm^3
Total extracellular concentration of osmolytes	Π_e	3.0×10^{-4} mol/cm^3
Mean organic osmolyte valency	z	-1.5

Table A3
Parameters of the Na/K-pump model [15].

Parameters	Symbols	Values
Intracellular ATP concentration	$[ATP]_{in}$	5.0×10^{-6} mol/cm^3
Intracellular ADP concentration	$[ADP]_{in}$	6.0×10^{-8} mol/cm^3
Intracellular concentration of phosphate ion	$[P_i]_{in}$	4.95×10^{-6} mol/cm^3
Rate constants of forward (f) and backward (b) reactions	f_{12}	2.5×10^{20} mol^{-3} cm^9 s^{-1}
	f_{23}	10^4 s^{-1}
	f_{34}^0	360 s^{-1}
	f_{45}	1.5×10^{13} mol^{-2} cm^6 s^{-1}
	f_{56}	2×10^9 mol^{-1} cm^3 s^{-1}
	f_{61}	1.15×10^4 s^{-1}
	b_{21}	424563 s^{-1}
	b_{32}	10^8 mol^{-1} cm^3 s^{-1}
	b_{43}^0	8.5×10^{12} mol^{-3} cm^9 s^{-1}
	b_{54}	2×10^8 mol^{-1} cm^3 s^{-1}
	b_{65}	30 s^{-1}
	b_{16}	6×10^{14} mol^{-2} cm^6 s^{-1}

Table B
First and second approximation versions of the model (*FAVM* and *SAVM* versions).

	Values of permeability parameters	
First approximation (*FAVM*)	$V/V_0 \leqslant V_{threshold}$	$V/V_0 > V_{threshold}$
	$P_K = P_K^0$ $P_{Cl} = P_{Cl}^0$ $P_X = 0$	$P_K = P_K^0 \times gain$ $P_{Cl} = P_{Cl}^0 \times gain$ $P_X = P_X^{RVD}$
Second approximation (*SAVM*) $\tau_{lag} = 1$ s	$V/V_0 \leqslant V_{threshold}$	$V/V_0 > V_{threshold}$ and $t > \tau_{lag}$
	$P_K = P_K^0$ $P_{Cl} = P_{Cl}^0$ $P_X = 0$	$P_K = P_K^0 \times \left((gain - 1) \times \left(\frac{V/V_0 - 1}{\mu} \right)^2 + 1 \right)$ $P_{Cl} = P_{Cl}^0 \times \left((gain - 1) \times \left(\frac{V/V_0 - 1}{\mu} \right)^2 + 1 \right)$ $P_X = P_X^{RVD} \times \left(\frac{V/V_0 - 1}{\mu} \right)^2$

500 and 600 mosmol/kgH$_2$O (Fig. C1). 3D confocal reconstructions of the cell volume in hypotonic medium is impossible for these cells because of the RVD reaction which is rapid and the cell volume is not stable enough in hypotonic medium (150 mosmol/kgH$_2$O) to get a 3D image. Cell volume (V) was calculated on the basis of 3D images as a sum of volumes of optical layers. Cell height along the z-axis was measured on the same cell. Relative cell volume (V/V_0) and cubed relative cell height (H/H_0)^3 were plotted versus the normalized inverse osmolality of the extracellular medium. As one can see the curves are almost identical (Fig. C2). On the basis of these results the assumptions that cell volume is proportional to the cell height cubed and that practically the whole cell ($\sim$90%) is osmotically active could be accepted.
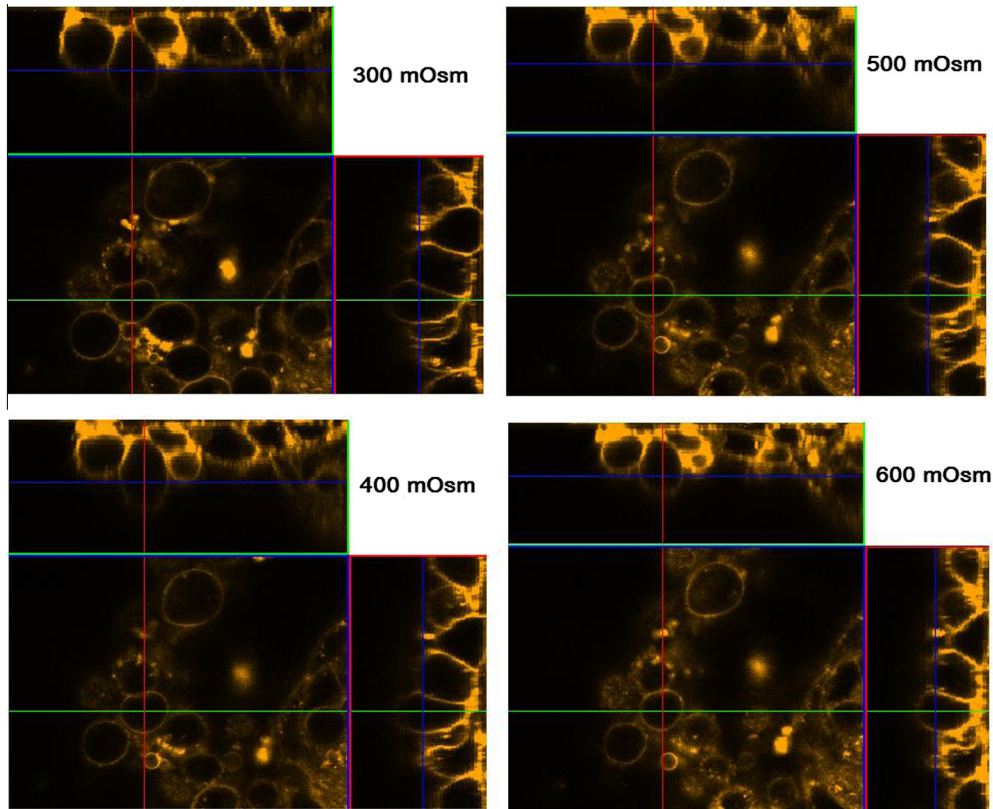
Fig. C1. 3D confocal reconstructions shown as orthogonal projections in solutions of different osmolalities. The crosshair points to the cell whose volume and height were measured.
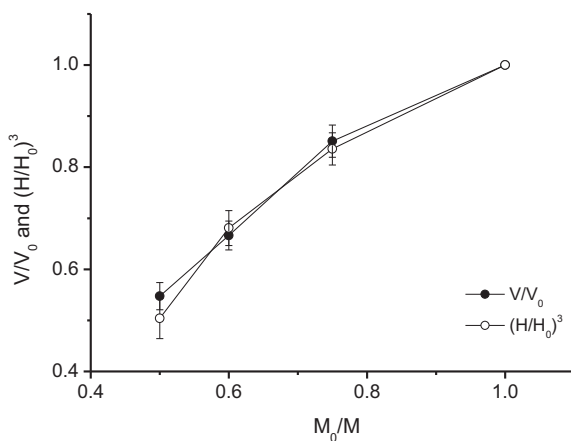

Fig. C2. Dependence of the relative cell volume and the relative cell height cubed on the normalized inverse osmolality of extracellular medium ($n = 5$), where $M_0 = 300$ mOsm/kg H_2O.

References

[1] C.M. Armstrong, The Na/K pump, Cl ion, and osmotic stabilization of cells, Proc. Natl. Acad. Sci. USA 100 (2003) 6257.

[2] J.K. Bubien, Epithelial Na$^+$ channel (ENaC), hormones, and hypertension, J. Biol. Chem. 285 (2010) 23527.

[3] I. Chapman, E. Johnson, J. Kootsey, Electrical and biochemical properties of an enzyme model of the sodium pump, J. Membr. Biol. 74 (1983) 139.

[4] C.L. Chou, M.J. Yu, E.M. Kassai, R.G. Morris, J.D. Hoffert, S.M. Wall, M.A. Knepper, Roles of basolateral solute uptake via NKCC1 and of myosin II in vasopressin-induced cell swelling in inner medullary collecting duct, Am. J. Physiol. Renal Physiol. 295 (2008) 192.

[5] A. Dyrda, U. Cytlak, A. Ciuraszkiewicz, A. Lipinska, A. Cueff, G. Bouyer, S. Egee, P. Bennekou, V.L. Lew, S.L.Y. Thomas, Local membrane deformations activate Ca^{2+} – dependent K$^+$ and anionic currents in intact human red blood cells, PLoS ONE 5 (2010) e9447.

[6] N.J. Ernest, A.K. Weaver, L.B. Van Duyn, H.W. Sontheimer, Relative contribution of chloride channels and transporters to regulatory volume decrease in human glioma cells, Am. J. Physiol. Cell Physiol. 288 (2005) 1451.

[7] J.A. Fraser, C.L. Huang, A quantitative analysis of cell volume and resting potential determination and regulation in excitable cells, J. Physiol. 559 (2004) 459.

[8] G. Frindt, L.G. Palmer, Ca-activated K channel in apical membrane of mammalian CCT, and their role in K secretion, Am. J. Physiol. 252 (1987) 458.

[9] G. Frindt, L.G. Palmer, Low-conductance K channels in apical membrane of rat cortical collecting tubule, Am. J. Physiol. 256 (1989) 143.

[10] L. Galizia, M.P. Flamenco, V. Rivarola, C. Capurro, P. Ford, Role of AQP2 in activation of calcium entry by hypotonicity: implications in cell volume regulation, Am. J. Physiol. Renal Physiol. 294 (2008) 582.

[11] J. Gifford, J. Galla, R. Luke, R. Rick, Ion concentrations in the rat CCD: differences between cell types and effect of alkalosis, Am. J. Physiol. 259 (1990) 778.

[12] D.E. Goldman, Potential, impedance and rectification in membranes, J. Gen. Physiol. 27 (1943) 37.

[13] J.M. Grunewald, R.W. Grunewald, R.K. Kinne, Ion content and cell volume in isolated collecting duct cells: effect of hypotonicity, Kidney Int. 44 (3) (1993) 509.

[14] J. Hernandez, J. Fischbarg, L.S. Liebovitch, Kinetic model of the effects of electrogenic enzymes on the membrane potential, J. Theor. Biol. 137 (1989) 113.

[15] J.A. Hernandez, S. Chifflet, Electrogenic properties of the sodium pump in a dynamic model of membrane transport, J. Membr. Biol. 176 (2000) 41.

[16] T. Hill, in: Free Energy Transduction in Biology, Academic Press, New York, 1977, pp. 1–32.

[17] A. Hodgkin, B. Katz, The effect of sodium ions on the electrical activity of the giant axon of the squid, J. Physiol. 108 (1949) 37.

[18] E. Hoffmann, I. Lambert, S. Pedersen, Physiology of cell volume regulation in vertebrates, Physiol. Rev. 89 (2009) 193.

[19] R. Jacob, D. Piwnica-Worms, C.R. Horres, M. Lieberman, Theoretical effects of transmembrane electroneutral exchange on membrane potential, J. Gen. Physiol. 83 (1984) 47.

[20] F.E. Karet, Disorders of water and acid-base homeostasis, Nephron Physiol. 118 (2011) 28.

[21] R. Kaunas, P. Nguyen, P. Usami, S. Chien, Cooperative effects of Rho and mechanical stretch on stress fiber organization, Proc. Natl. Acad. Sci. USA 102 (2005) 15895.

[22] F. Lang, G.L. Busch, M. Ritter, H. Volkl, S. Waldegger, E. Gulbins, D. Haussinger, Functional significance of cell volume regulatory mechanisms, Physiol. Rev. 78 (1998) 247.

[23] S. Lee, Z. Shen, D. Robinson, S. Briggs, R. Firtel, Involvement of the cytoskeleton in controlling leading edge function during chemotaxis, Mol. Biol. Cell 21 (2010) 1810.

[24] J. Legato, M.A. Knepper, R.A. Star, R. Mejia, Database for renal collecting duct regulatory and transporter proteins, Physiol. Genomics 13 (2003) 179.

[25] R.B. Moreton, An investigation of the electrogenic sodium pump in snail neurons, using the constant-field theory, J. Exp. Biol. 51 (1969) 181.

[26] S. Muto, Potassium transport in the mammalian collecting duct, Physiol. Rev. 81 (2001) 85.

[27] S. Nielsen, J. Frokiaer, D. Marples, T.H. Kwon, P. Agre, M.A. Knepper, Aquaporins in the kidney: from molecules to medicine, Physiol. Rev. 82 (2002) 205.

[28] C. Pappas, B. Koeppen, Electrophysiological properties of cultured outer medullary collecting duct cells, Am. J. Physiol. 263 (1992) 1004.

[29] M.C. Reif, S.L. Troutman, J.A. Schafer, Sodium transport by rat cortical collecting tubule. Effects of vasopressin and desoxycorticosterone, J. Clin. Invest. 77 (1986) 1291.

[30] E. Solenov, H. Watanabe, G.T. Manley, A.S. Verkman, Sevenfold-reduced osmotic water permeability in primary astrocyte cultures from AQP-4-deficient mice, measured by a fluorescence quenching method, Am. J. Physiol. Cell Physiol. 286 (2004) 426.

[31] E.I. Solenov, G.S. Baturina, L.E. Katkova, Role of water channels in the regulation of the volume of principal cells of rat kidney collecting ducts in hypoosmotic medium, Biofizika 53 (2008) 684.

[32] E.I. Solenov, A.V. Ilyaskin, G.S. Baturina, D.A. Medvedev, A.P. Ershov, D.I. Karpov, A mathematical model of the cell volume regulation in a hypotonic medium, Dokl. Biol. Sci. 437 (2011) 79.

[33] K. Strange, Cellular volume homeostasis, Adv. Physiol. Edu. 28 (2004) 155.

[34] G. Tamma, G. Procino, A. Strafino, E. Bononi, G. Meyer, M. Paulmichi, V. Formoso, M. Svelto, G. Valenti, Hypotonicity induces aquaporin-2 internalization and cytosol-to-membrane translocation of ICln in renal cells, Endocrinology 148 (2007) 1118.

[35] P. Teng-umnuay, J.W. Verlander, W. Yuan, C.C. Tisher, K.M. Madsen, Identification of distinct subpopulations of intercalated cells in the mouse collecting duct, J. Am. Soc. Nephrol. 7 (1996) 260.

[36] S.M. Wall, M.P. Fischer, P. Mehta, K.A. Hassell, S.J. Park, Contribution of the Na^+-K^+-$2Cl^-$ cotransporter NKCC1 to Cl^- secretion in rat OMCD, Am. J. Physiol. Renal Physiol. 280 (2001) 913.

[37] W. Wang, S.C. Hebert, G. Giebisch, Renal K^+ channels: structure and function, Annu. Rev. Physiol. 59 (1997) 413.

[38] L. Wang, G. Ding, Q. Gu, W. Schwarz, Single-channel properties of a stretch-sensitive chloride channel in the human mast cell line HMC-1, Eur. Biophys. J. 39 (2010) 757.

[39] A.M. Weinstein, Analysis of volume regulation in an epithelial cell model, Bull. Math. Biol. 54 (1992) 537.

[40] A.M. Weinstein, Modeling epithelial cell homeostasis: steady-state analysis, Bull. Math. Biol. 61 (1999) 1065.

[41] A.M. Weinstein, A mathematical model of rat cortical collecting duct: determinants of the transtubular potassium gradient, Am. J. Physiol. 280 (2001) 1072.

[42] D. Whitley, A genetic algorithm tutorial, Stat. Comput. 4 (1994) 65.